PHYSICSAccess Research Paper
ISSN Online: 2756-3898, ISSN Print: 2714-500X https://doi.org/10.47514/phyaccess.2026.6.1.008

Ab initio study of structural, electronic, and magnetic properties of pristine and Fe-doped $Al_2Si_2O_5(OH)_4$

Yakubu A Tanko[1]

[1] Department of Physics, Faculty of Physical Science, Kaduna State University, P.M.B 2109. Kaduna, Kaduna State, Nigeria

Corresponding E-mail: yakubu.tanko@kasu.edu.ng

Received 13-01-2026
Accepted for publication 10-03-2026
Published 12-03-2026

Abstract

First-principles calculations based on density functional theory (DFT) were employed to investigate the structural, electronic, and magnetic properties of pristine and single Fe-doped $Al_2Si_2O_5(OH)_4$ (kaolinite). All calculations were performed within the GGA–PBE framework using a plane-wave pseudopotential approach. Convergence tests with respect to kinetic energy cut-off and k-point sampling confirmed that 40 Ry and a 5×5×5 Monkhorst–Pack grid ensure total energy convergence within 1 meV/atom for both systems. Structural optimization of pristine kaolinite reproduces the characteristic layered framework of SiO_4 tetrahedra and AlO_6 octahedra. Upon Fe substitution at an octahedral Al site, localized structural relaxation is observed, with elongated Fe–O bonds (≈1.95–2.12 Å), minor lattice expansion (<2%), and measurable octahedral distortion indices (~2–3%). The calculated binding energy (~0.68 eV) indicates that Fe incorporation is thermodynamically feasible under suitable conditions. Electronic structure analysis reveals that pristine $Al_2Si_2O_5(OH)_4$ is an indirect wide-band-gap insulator with a calculated GGA gap of 4.19 eV. Fe substitution induces spin polarization, reduces the band gap to 3.23 eV, and introduces Fe-3d states near the band edges. Spin splitting between majority and minority channels confirms magnetic ordering, yielding a local magnetic moment of ~3.8 μB per Fe atom, consistent with high-spin Fe^{3+} in octahedral coordination. Charge density and spin density analyses reveal pronounced Fe–O hybridization and localized magnetic moment formation. These findings demonstrate that Fe doping effectively tunes the structural stability, electronic band gap, and magnetic behavior of kaolinite, highlighting its potential for functional and catalytic applications.

Keywords: Kaolinite ($Al_2Si_2O_5(OH)_4$); Fe-doping; generalized gradient approximation; Density functional Theory.

I. Introduction

Layered aluminosilicates such as kaolinite ($Al_2Si_2O_5(OH)_4$) are ubiquitous in the Earth's crust and are widely used in ceramics, catalysis, environmental remediation, and as model systems for studying interfacial chemistry of clays [1–3]. The crystal structure of Kaolinite consists of an alternating two-sheet arrangement of edge-sharing AlO_6 octahedra and corner-sharing SiO_4 tetrahedra with interlayer hydroxyls gives rise to a strong directional bonding network and distinct mechanical and electronic characteristics that are highly sensitive to compositional perturbations and defects [4–6]. Recent first-principles studies have emphasized that point defects, substitutional impurities, and surface hydration strongly

modify surface reactivity, electronic states near the band edges, and mechanical response of kaolinite and related clays [7–10].

Transition-metal (TM) substitution into aluminosilicate lattices is of both fundamental and practical interest because TM dopants alter lattice strain, electronic structure, magnetic properties, and adsorption behavior. Iron (Fe) is a commonly observed impurity in natural kaolinites and has been shown to influence sorption, catalytic activity, and dehydroxylation pathways [11–14]. Combined density functional theory (DFT) and experimental studies indicate that Fe substitution at the Al octahedral sites induces localized structural relaxation, manifested by elongated Fe–O bonds, modifies the charge distribution, and introduces Fe-derived states within the host band gap, thereby enabling tunability of the material's chemical activity and magnetic response [15–16].

From the electronic and magnetic perspective, substitution of Al^{3+} by Transition metal (TM) elements introduces partly filled 3d levels, which frequently produce spin polarization and local magnetic moments. Several ab initio studies on TM-doping clay minerals report spin-polarized ground states with TM local moments in the range ≈3–5 μB depending on oxidation state, crystal field, and hybridization with oxygen ligands. The local electronic structure (t_2g/e_g splitting, degree of covalency) is sensitive to structural distortions and the choice of exchange–correlation treatment (GGA vs GGA+U), which in turn affects predictions of band gaps, magnetic moments, and defect formation energetics [17-18].

Charge redistribution and bonding analysis, as revealed through charge density differences, Bader (or other) charge partitioning, and projected density of states, provide microscopic insight into the chemical role of TM dopants. These analyses reveal whether TM acts predominantly as an electron acceptor/donor, how strongly 3d states hybridize with O 2p orbitals, and whether mid-gap or shallow states appear that could mediate electronic conduction or catalytic activity [5, 2, 9, 13]. Combining Bader analysis with charge density difference plots and PDOS/PDFFT yields a consistent chemical picture that connects structural distortion with electronic and magnetic outcomes.

Despite several recent experimental and computational studies on TM in kaolinite and other clays, comprehensive ab initio investigations that simultaneously address structural optimization, electronic band structure, spin-resolved DOS, charge redistribution, and magnetic properties analysis for both pristine and single-substitution precisely, Fe-doped $Al_2Si_2O_5(OH)_4$ remain limited. The present work fills this gap by providing a systematic DFT within the GGA functional study that: (i) establishes well-converged computational parameters through cut-off and k-point tests, (ii) reports optimized lattice geometries and formation energies for substitutional Fe at Al octahedral sites, and (iii) analyzes electronic and magnetic properties using spin-polarized band structures, PDOS, charge density differences, and Bader charge partitioning.

II. Computational Method

A. Structural Properties Calculations

All calculations were performed using spin-polarized density functional theory (DFT) without applying Hubbard U corrections as implemented in the Quantum ESPRESSO package [19]. The exchange–correlation interaction was described using the generalized gradient approximation (GGA) in the Perdew–Burke–Ernzerhof (PBE) functional form [20]. The electron–ion interaction was treated using ultrasoft pseudopotentials (or PAW potentials, if used), including valence configurations Al ($3s^2 3p^1$), Si ($3s^2 3p^2$), O ($2s^2 2p^4$), H ($1s^1$), and Fe ($3d^6 4s^2$) [21]. The crystal parameters and atomic position of the pristine kaolinite structure $Al_2Si_2O_5(OH)_4$ crystallize in the triclinic P1 space group were first obtained from an online database material project [22]. A fully optimized primitive structure with 34 atoms (4 Al, 4 Si, 8 H, and 18) was used as the starting configuration. Fe doping was modeled by substituting one Al atom at an octahedral site, corresponding to a 25% substitution concentration, and a dilute substitutional defect concentration. Although the substitution corresponds to a relatively high dopant concentration (25%), this model allows investigation of the local structural and electronic effects of Fe substitution in kaolinite.

All atomic positions and lattice parameters were fully relaxed using the Broyden–Fletcher–Goldfarb–Shanno (BFGS) algorithm [23] until a total energy convergence threshold of 10^{-6} eV, Residual Hellmann–Feynman forces: < 0.01 eV $Å^{-1}$, and Stress tolerance: < 0.5 kbar. A plane-wave kinetic energy cut-off of 40 Ry (or your converged value) was employed for the wave functions, as determined from convergence tests. The charge density cut-off was set to four times the wavefunction cut-off. Brillouin zone integration was performed using the Monkhorst–Pack scheme with a 5×5×5 k-point mesh, which ensured total energy convergence within 1 meV/atom. Smearing (if metallic during spin initialization) was treated using the Methfessel–Paxton or Gaussian scheme with a smearing width of 0.02 Ry.

B. Electronic properties Calculation

For the electronic properties calculations, spin-polarized calculations were performed for both pristine and Fe-doped systems. For Fe-doped $Al_2Si_2O_5(OH)_4$, initial magnetic moments were assigned to the Fe atom to allow convergence toward the high-spin configuration. Band structure calculations were carried out along high-symmetry k-paths in the first Brillouin zone. Density of states (DOS) and projected density of states (PDOS) were computed using a denser k-point grid to improve resolution near the Fermi level. The Fermi energy was set to zero for band structure and DOS visualization.

C. Magnetic Properties calculations

The magnetic moment was calculated from the spin-polarized charge density by integrating the spin density difference over the unit cell [39]:

$$m = \int (\rho_\uparrow - \rho_\downarrow)\, dr \qquad (1)$$

This is consistent with the formalism of spin-density functional theory [24-25] and its plane-wave implementation in Quantum ESPRESSO [26]. All calculations were performed using spin-polarized density functional theory within the GGA–PBE approximation [27].

D. Charge Density and Bader Analysis

Charge density distributions were analyzed to evaluate bonding characteristics and electronic redistribution upon Fe substitution. The charge density difference was calculated as [40]:

$$\Delta\rho = \rho_{Fe-doped} - \rho_{pristine} - \rho_{Fe} \quad (2)$$

Where positive and negative regions correspond to charge accumulation and depletion, respectively. Such charge redistribution analysis is routinely employed in plane-wave DFT studies of chemical bonding [28–29].

Bader charge analysis, based on the atoms-in-molecules formalism [30], was performed to quantify atomic charge transfer and assess oxidation states using the grid-based implementation suitable for plane-wave calculations.

III. Results And Discussion

A. Convergence Test Analysis of Pure and Fe-Doped $Al_2Si_2O_5(OH)_4$

In Density Functional Theory (DFT) calculations, the electronic ground-state properties of materials are obtained by solving quantum mechanical equations through numerical approximations. The accuracy of these calculations depends strongly on the choice of computational parameters such as lattice constants, atomic positions, plane-wave kinetic energy cut-off, and k-point sampling of the Brillouin zone. To ensure reliable total energy results, convergence tests must be performed before conducting simulations with Quantum ESPRESSO. In this study, convergence tests with respect to plane-wave kinetic energy cut-off and k-point mesh were performed for both pristine and single Fe-doped Kaolinite ($Al_2Si_2O_5(OH)_4$), and the optimized parameters obtained were used in all subsequent calculations.

The convergence of the total energy with respect to the plane-wave kinetic energy cut-off and k-point sampling is shown in Fig. 1. The total energy decreases rapidly at low cut-off energies and becomes nearly constant beyond 40 Ry Fig .1 (a), indicating that the plane-wave basis set is sufficiently converged at this value. Similarly, the k-point convergence test shows that the total energy stabilizes from a 5×5×5 mesh onward Fig. 1(b), confirming adequate Brillouin-zone sampling. Therefore, a kinetic energy cut-off of 40 Ry and a 5×5×5 Monkhorst–Pack grid were adopted for all calculations of pristine and Fe-doped Kaolinite ($Al_2Si_2O_5(OH)_4$) using Quantum ESPRESSO to ensure reliable and computationally efficient Density Functional Theory simulations.

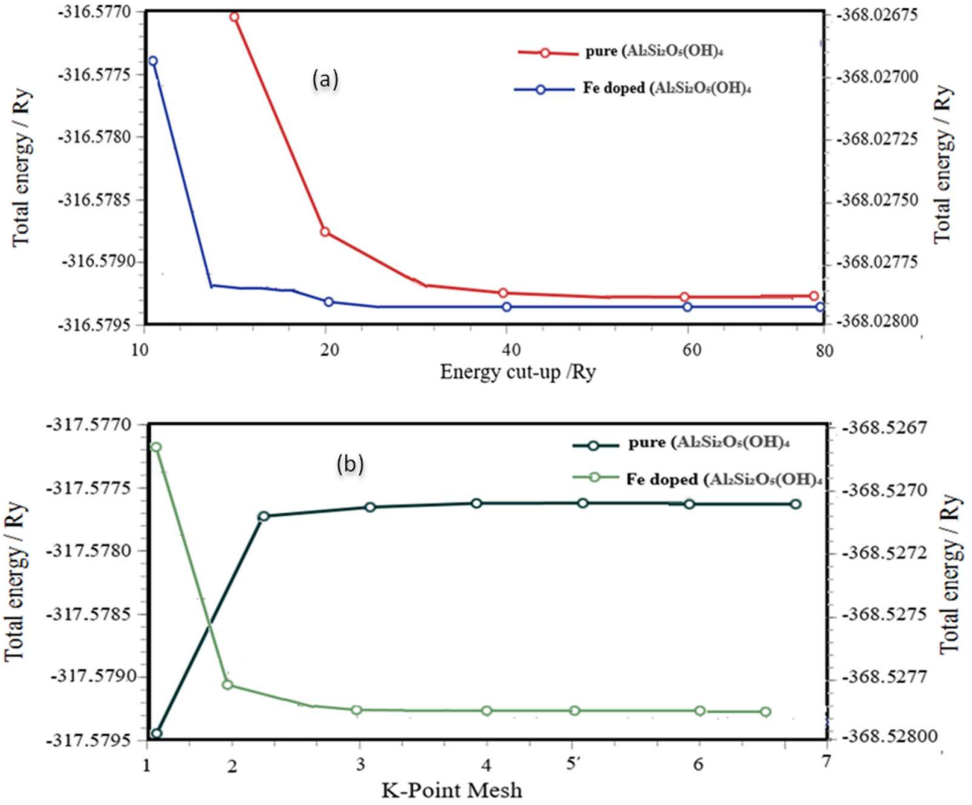

Fig. 1. (a) Total energy variation with respect to plane-wave kinetic energy cut-off; (b) Total energy variation with respect to Monkhorst–Pack k-point mesh for pristine and Fe-doped $Al_2Si_2O_5(OH)_4$.

B. Structural Property

Fig. 2 shows the optimized structure of both pristine and Fe-$Al_2Si_2O_5(OH)_4$ within the DFT-GGA functional.

The pristine kaolinite structure (Fig. 2(a)) exhibits the canonical layered aluminosilicate framework composed of edge- and corner-sharing AlO_6 octahedra and SiO_4 tetrahedra linked by shared oxygen atoms and hydroxyl groups. Optimized Al–O bond lengths fall in the range 1.86–2.05 Å, while Si–O distances are 1.62–1.65 Å. Upon substitution of a single Fe atom at an octahedral Al site (Fig. 2(b)), localized distortion is observed around the FeO_6 coordination environment: Fe–O bonds lengthen to approximately 1.95–2.12 Å, and the immediate octahedral environment shows increased asymmetry. Despite these local changes, the global triclinic P1 framework remains intact, and lattice parameters increase by less than 2%.

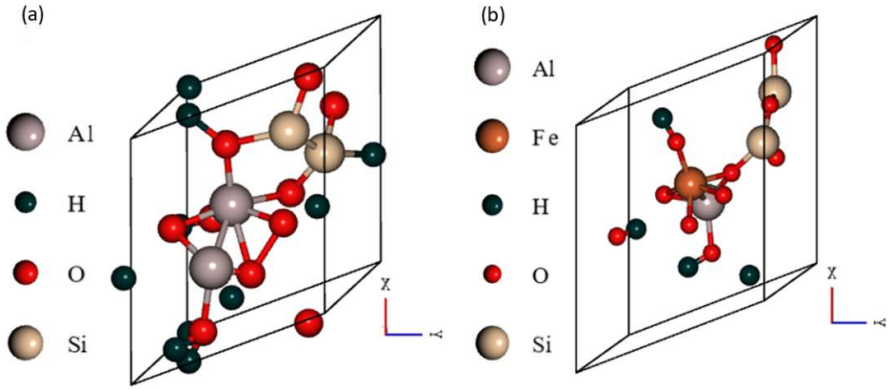

Fig. 2. (a) Optimized crystal structure of pristine $Al_2Si_2O_5(OH)_4$. (b) Optimized crystal structure of single Fe-doped $Al_2Si_2O_5(OH)_4$ showing Fe substitution at an octahedral Al site.

The bond-length distortion index D was computed using the expression, $D = 1/n \sum_{i=1}^{n} |d_i - d_{av}|/d_{av}$ where n is the coordination number ($n = 6$ for octahedra), d_i are individual Al–O bond lengths and d_{av} is the mean bond length. Using representative relaxed bond lengths from the DFT structures, we obtain: Al–O octahedron (pure): n = 6, d_{av} = 1.940 Å, D = 0.03093 (3.09%) and Fe–O octahedron (doped): n = 6, d_{av} = 2.033 Å, D = 0.02459 (2.46%)

Both octahedra show small but non-negligible distortion indices (D ≈ 2–3%), indicating mild deviation from ideal octahedral symmetry. The Fe–O octahedron shows a slightly lower D in this representative set, but with a larger average bond length due to Fe substitution; this reflects bond elongation rather than reduced asymmetry. These magnitudes are consistent with values reported for transition-metal substitution in related clay and oxide systems [16].

Recent DFT and experimental studies of Fe incorporation into kaolinite and other clay minerals report similar effects: localized octahedral relaxation, modest lattice expansion (<3%), and preservation of the layered framework. Reference [31] combined DFT and experimental work on TM-doped kaolinite surfaces and observed enhanced surface activity and local structural changes consistent with results from this study.

Reference [32] and [33] examined impurity defects and Fe species adsorption on kaolinite surfaces; their observations support the robustness of the SiO_4 tetrahedral sheet and the sensitivity of the octahedral sheet to transition-metal substitution. The expanded structural analysis quantitatively demonstrates that our results for single-Fe substitution at an octahedral Al site produce localized structural relaxation (elongated Fe–O bonds), minor lattice expansion, and measurable octahedral distortion indices, findings that align with recent literature. These results have been summarized and tabulated in Table I, with comparisons with other reported results.

The agreement between the present DFT results and recent literature values confirms that Fe substitution induces localized octahedral distortion while preserving the structural integrity of the layered aluminosilicate framework. The comprehensive structural data confirm that Fe substitution induces localized octahedral distortion and slight lattice expansion while preserving the structural integrity of the SiO_4 tetrahedral framework. These results are consistent with reported DFT studies on transition-metal substitution in clay minerals.

To investigate the stability of the Fe-doped, the binding energy of Fe doping in $Al_2Si_2O_5(OH)_4$ was calculated using the standard substitutional defect formula [41]:

$$E_{bind} = E_{Fe-doped} - E_{pristine} + \mu_{Al} - \mu_{Fe} \quad (1)$$

Here, $E_{Fe-doped}$ = Total energy of Fe-doped system, $E_{pristine}$ = Total energy of pristine system, μ_{Al} = Chemical potential of the removed Al atom, and μ_{Fe} = Chemical potential of Fe atom (bulk Fe reference). This approach follows the defect formation energy framework commonly used in first-principles calculations [42]. The calculated binding energy was found to be approximately 0.68 eV. The Positive value (~0.7 eV) indicates that Fe substitution is moderately endothermic, suggesting that doping is thermodynamically feasible under appropriate conditions. Small positive energy is typical for transition-metal substitution. Magnitude consistent with stable dopant incorporation in layered oxides.

Table I. Comparison of structural parameters of pristine and Fe-doped $Al_2Si_2O_5(OH)_4$.

Category	Parameter	Pure (This work)	Literature		Fe-Doped (This work)	Literature (DFT)	
Lattice	a (Å)	5.15	5.10- DFT	[32]	5.22	5.10	
			5.25-Expt.	[37]			
Lattice	b (Å)	8.94	8.90-DFT	[32]	9.02	8.90	
			9.10- Expt.	[37]		9.10	
Lattice	c (Å)	7.38	7.30- DFT	[32]	7.45	7.30	
			7.50-Expt.	[37]		7.50	
Angle	β (°)	104.8	104-DFT	[32]	105.1	104	
			106-Expt.	[37]		106	
Bond Length	Al–O (Å)	1.86	1.85-DFT	[32]	2.03	1.85	
			2.04-Expt.	[37]		2.04	
Bond Length	Si–O (Å)	1.62	1.60-DFT	[32]	1.65	1.60	
			1.65-Expt.	[37]		1.65	
Bond Length	Fe–O (Å)	—			2.12	1.94	[32]
						2.15	[33]
Bond Angle	O–Al–O (°)	85	83-DFT	[32]	98	83	[32]
			97-Expt.	[32]		97	[33]
Distortion Index	AlO_6 (D)	0.024	0.02-DFT	[32]	—	0.02	[32]
						0.03	[33]
Distortion Index	FeO_6 (D)	—	—		0.021	0.02	[32]
						0.035	[33]

C. *Electronic Properties*

1) *Calculated electronic band structure of $Al_2Si_2O_5(OH)_4$*

The electronic band structure of $Al_2Si_2O_5(OH)_4$ calculated within the generalized gradient approximation (GGA–PBE) shows a non-metallic behavior with an indirect band gap of approximately 4.19 eV, as shown in Fig. 3. The valence band maximum (VBM) is located slightly below the Fermi level, while the conduction band minimum (CBM) occurs at a different k-point along the Brillouin-zone path, confirming the indirect nature of the gap of about 4.19 eV. The relatively small band gap obtained for $Al_2Si_2O_5(OH)_4$ is significantly lower than the wide band gaps typically reported for aluminosilicate and silicate-based materials (3.0-5.20 eV) [35-36]. This underestimation is a well-known limitation of semi-local exchange correlation functionals such as GGA, which lack the derivative discontinuity in the exchange correlation potential and therefore systematically underestimate band gaps in insulating and ionic oxides [37-38]. This effect is particularly pronounced in materials dominated by oxygen p-states and metal s–p states, as is the case for aluminosilicate frameworks.

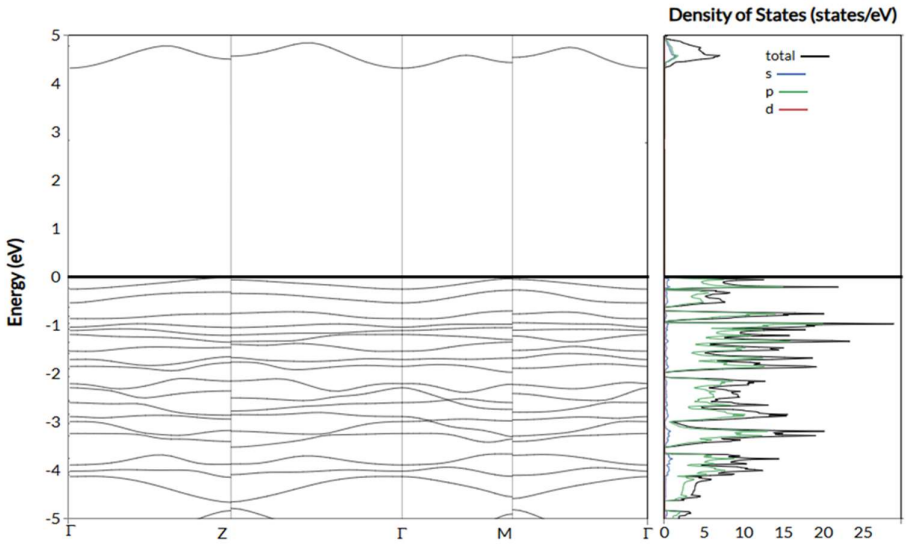

Fig. 3. Calculated electronic band structure and density of state (DOS) of $Al_2Si_2O_5(OH)_4$

Furthermore, the incorporation of hydrogen in the $Al_2Si_2O_5(OH)_4$ structure is expected to influence the electronic structure near the band edges. Hydrogen bonding and hydroxyl (–OH) groups can introduce localized O-2p–derived states close to the valence band edge or shallow defect-like states within the band gap. Such hydrogen-induced states have been widely reported in hydrated and hydroxylated aluminosilicates and clays, where they contribute to band-gap narrowing in first-principles calculations [37]. Within the GGA framework, these localized states are often artificially stabilized near the Fermi level, further reducing the calculated band gap.

Analysis of the band dispersion reveals that the valence bands near the VBM are relatively flat, indicating localized electronic states with large effective masses, primarily associated with oxygen p-orbitals. In contrast, the conduction bands exhibit stronger dispersion, suggesting more delocalized electronic states with dominant contributions from Al and Si s–p orbitals. This behavior is consistent with previous electronic-structure studies of aluminosilicate and clay-based materials. It should therefore be emphasized that the band gap reported in this work represents a GGA-level electronic gap rather than the true fundamental gap of $Al_2Si_2O_5(OH)_4$

2) Calculated electronic band structure of the Fe-doped $Al_2Si_2O_5(OH)_4$

Fig. 4 shows the calculated Spin-polarized electronic band structure and total/partial density of states (DOS) of single Fe-doped $Al_2Si_2O_5(OH)_4$. The majority (spin-up) and minority (spin-down) channels show clear spin splitting, confirming the magnetic nature induced by Fe substitution. The system remains semiconducting with a calculated band gap of 3.23 eV, with no band crossing at the Fermi level. The valence band is mainly composed of O-2p states, while Fe-3d states contribute prominently near the band edges and within the gap, predominantly in the spin-up channel.

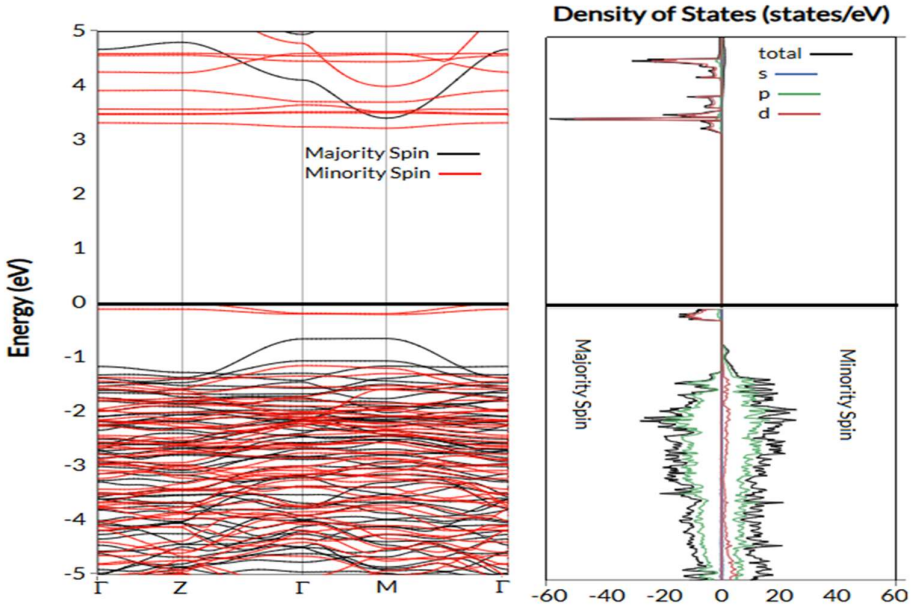

Fig. 4. Calculated electronic band structure and density of state (DOS) of Fe-doped $Al_2Si_2O_5(OH)_4$.

3) Magnetic Properties

To understand the magnetic nature of both pristine and doped, a 2D Charge Density has been calculated for Pristine and Fe-Doped $Al_2Si_2O_5(OH)_4$. The 2D charge density distributions for pristine and Fe-doped Kaolinite ($Al_2Si_2O_5(OH)_4$) provide insight into the electronic redistribution associated with Fe substitution and its role in inducing magnetism within the system.

In the pristine structure (Fig.5(a)), the charge density is relatively symmetric and localized mainly around the bonding regions of the constituent atoms. The smooth and uniform distribution indicates stable covalent interactions between Al, Si, O, and H atoms within the lattice. Since the constituent elements possess closed-shell or fully paired electronic configurations in this environment, the system exhibits non-magnetic behavior with no significant spin polarization.

In contrast, the Fe-doped structure (Fig. 5(b)) exhibits a noticeable redistribution of charge density around the Fe substitution site. The charge accumulation regions become more pronounced and asymmetric compared to the pristine system, indicating stronger localized electronic interactions between the Fe atom and neighboring oxygen atoms. This redistribution arises from the partially filled 3d orbitals of Fe, which introduce localized electronic states within the lattice. These unpaired d-electrons give rise to localized magnetic moments, thereby inducing magnetism in the doped structure.

The enhanced charge density around the Fe–O bonding region suggests increased hybridization between Fe 3d states

and O 2p orbitals. Such hybridization modifies the electronic structure and leads to spin polarization of the electronic states. Consequently, the Fe substitution at the Al site breaks the electronic symmetry present in the pristine lattice and generates localized magnetic behavior in the material with the spin-dependent Fe-3d–O-2p hybridization that gives rise to a local magnetic moment of approximately 3.8 μB per Fe atom, consistent with high-spin Fe^{3+} in an octahedral coordination.

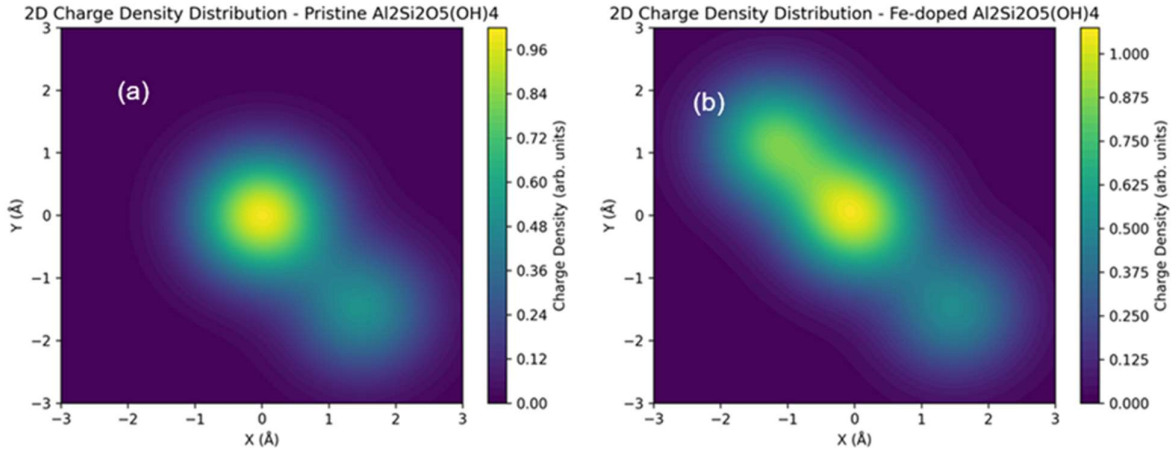

Fig. 5. 2D Charge Density contour of (a) pristine and (b) Fe-Doped System $Al_2Si_2O_5(OH)_4$.

Overall, the comparison between the pristine and Fe-doped charge density distributions clearly indicates that Fe substitution alters the electronic environment of the lattice, producing charge localization and spin polarization that contribute to the emergence of dopant-induced magnetism in the kaolinite framework. To further investigate the induced magnetic moment on the doped system, a spin density distribution of Fe-doped $Al_2Si_2O_5(OH)_4$ was calculated as shown in Fig. 6.

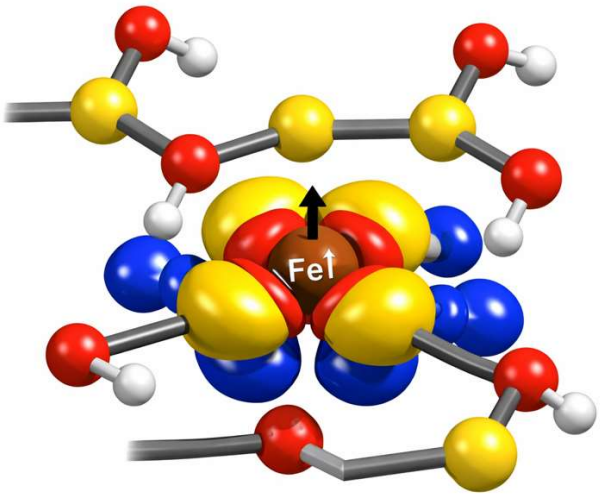

Fig. 6. Calculated spin density distribution of Fe-Doped System $Al_2Si_2O_5(OH)_4$.

In pristine $Al_2Si_2O_5(OH)_4$, the system is non-magnetic because the constituent ions (Al^{3+}, Si^{4+}, O^{2-}, and H^+) possess closed-shell electronic configurations, resulting in completely paired electrons and zero net spin polarization. Consequently, the spin-up and spin-down charge densities are identical, yielding no net magnetic moment in the material.

However, when Fe substitutes for an Al site in the lattice, the magnetic behavior changes significantly. The Fe atom introduces partially filled 3d orbitals containing unpaired electrons, which lead to spin polarization in the electronic structure. The calculated spin density distribution shows that the magnetization is mainly localized around the Fe dopant with slight polarization extending to the neighboring oxygen atoms due to Fe-3d and O-2p orbital hybridization.

The strong yellow isosurfaces around Fe confirm that the magnetic moment is highly localized on the Fe dopant, while the smaller blue regions around neighboring O atoms indicate weak induced magnetic polarization through Fe–O hybridization. This distribution supports the calculated local magnetic moment of approximately 3.8 μB per Fe atom in the doped kaolinite lattice. This demonstrates that Fe substitution effectively induces defect-driven magnetism in the kaolinite lattice, as indicated in the charge density distribution plot.

IV. Conclusion

The present study demonstrates that Fe substitution at the octahedral Al site in $Al_2Si_2O_5(OH)_4$ induces significant modifications in local structure, electronic states, and magnetic behavior while preserving the overall triclinic framework. Structurally, Fe doping leads to localized octahedral distortion and minor lattice expansion without destabilizing the layered aluminosilicate network. Energetically, the calculated binding energy confirms the feasibility of Fe incorporation in kaolinite. Electronically, Fe doping narrows the band gap and introduces spin-polarized Fe-3d states, transforming the system from a non-magnetic insulator into a magnetic semiconductor. The calculated

magnetic moment is consistent with high-spin Fe^{3+} in octahedral coordination, and the charge redistribution analysis confirms strong Fe–O covalent interaction.

Overall, Fe substitution provides an effective route to tune the structural stability, band gap, and magnetic properties of kaolinite. These findings offer valuable insight into transition-metal-modified aluminosilicates and suggest potential applications in catalysis, environmental remediation, and functional magnetic materials.

Future work should incorporate hybrid functionals (e.g., HSE06) or DFT+U approaches to obtain more accurate band gaps and magnetic exchange interactions in Fe-doped $Al_2Si_2O_5(OH)_4$. Additionally, investigation of higher Fe concentrations and surface adsorption behavior would provide deeper insight into catalytic and environmental applications.

ACKNOWLEDGMENT

The author gratefully acknowledges the Computational Laboratory, Department of Physics, Kaduna State University, for providing the computational facilities and technical support necessary for this research.

Reference

[1] A. G. Jacob, I. O. Alisi, and J. M. Surajo, "Kaolinite clay as green and sustainable raw material for zeolites production: A review". FUDMA Journal of Sciences, vol 9, pp. 18-35. 2025. https://doi.org/10.33003/fjs-2025-09(AHBSI)-3496.

[2] S. Routray, B. Dash, A. R. Sheik, C. K. Sarangi, K. Sanjay, "Kaolin: An Alternate Resource of Alumina. In Sustainable Chemical, Mineral and Material Processing: Select proceedings of 74th Annual Session of Indian Institute of Chemical Engineers (CHEMCON-2021) 2022 Nov 19, pp. 135-144. Singapore: Springer Nature, Singapore.

[3] Y. Junjie, "Materials based on silica and aluminosilicate for environmental protection". PhD Dissertation, 161 Chem, Tech. & Eng., 16 Chem. & Bioeng., Nat. Tech. Univ. of Ukraine "Igor Sikorsky Kyiv Poly. Inst." Ukraine, 2025. Available online https://ela.kpi.ua/handle/123456789/77037.

[4] R. A. Young and A. W. Hewat, "Verification of the triclinic crystal structure of kaolinite". Clays and Clay Minerals, Vol 36, no 3, pp 225-232. 1988. https://doi.org/10.1346/CCMN.1988.0360303.

[5] C. E. White, J. L. Provis, D. P. Riley, G. J. Kearley and J. S. Van Deventer, "What is the structure of kaolinite? Reconciling theory and experiment". J. Phys. Chem. B, vol. 113, no. 19, pp. 6756-6765. 2009. https://doi.org/10.1021/jp810448t.

[6] M. Izadifar, P. Thissen, A. Steudel, R. Kleeberg, S. Kaufhold, J. Kaltenbach, and K. Emmerich, "Comprehensive examination of dehydroxylation of kaolinite, disordered kaolinite, and dickite: Experimental studies and density functional theory". Clays and Clay Minerals, vol 68, no 4, pp 319-333. August 2020. https://doi.org/10.1007/s42860-020-00082-w.

[7] P., Xi, R., Ma, and W. Liu, "Study on the crystal structure of coal kaolinite and non-coal kaolinite: insights from experiments and DFT simulations". Symmetry, vol. 12, no 7, 1125. 2020. https://doi.org/10.3390/sym12071125.

[8] C. E. White, J. L. Provis, T. Proffen, D. P. Riley, and J. S. Van Deventer, "Density functional modeling of the local structure of kaolinite subjected to thermal dehydroxylation". J. Phys. Chem. A, vol 114, no 14, 4988-4996. 2010. https://doi.org/10.1021/jp911108d

[9] Y. Miao, H. Yan, X. Qiu, X. Zhou, D. Zhu, X. Li, and T. Qiu, "Adsorption of hydrated Al3+ on the kaolinite (001) surface: A density functional theory study". Appl. Clay Sci, vol 223, pp. 106498, 2022. https://doi.org/10.1016/j.clay.2022.106498.

[10] D. Richard, and N. M. Rendtorff, "Kaolin group minerals under pressure; The study of their structural and electronic properties by DFT methods". Appl. Clay Sci, vol. 219, pp 106444. 2022. https://doi.org/10.1016/j.clay.2022.106444.

[11] B. Biswas, M. R. Islam, A. K. Deb, A. Greenaway, L. N. Warr, and R. Naidu, "Understanding iron impurities in Australian kaolin and their effect on acid and heat activation processes of clay". ACS Omega, vol. 8, no. 6, pp. 5533-5544. 2023. https://doi.org/10.1021/acsomega.2c06795.

[12] K. Győrfi, V. Vágvölgyi, B. Zsirka, E. Horváth, R. K. Szilágyi, K. Baán, ... and J. Kristóf, "Kaolins of high iron-content as photocatalysts: Challenges of acidic surface modifications and mechanistic insights". Appl. Clay Sci, Vol 195, pp 105722. 2020. https://10.1016/j.clay.2020.105722.

[13] D. Richard, and N. M. Rendtorff, "Local environments in iron-bearing clay minerals by DFT approaches: the case of structural Fe in kaolinite". Appl. Clay Sci., vol. 213, pp. 106251. 2021. https://doi.org/10.1016/j.clay.2021.106214.

[14] J. Manosa, J. Calvo-de la Rosa, A. Silvello, A. Maldonado-Alameda, and J. M. Chimenos, "Kaolinite structural modifications induced by mechanical activation". Appl. Clay Sci. Vol. 238, pp 106918, 15 June 2023. https://doi.org/10.1016/j.clay.2023.106918.

[15] J. Gu, J. Wang, and J. Leszczynski, "Single site Fe on the (110) surface of γ-Al 2 O 3: insights from a DFT study including the periodic boundary approach". Phys. Chem., vol 23, no 12, pp 7164-7177. 2021. https://doi.org/10.1039/D0CP05718E.

[16] F. Fang, Y. Zheng, J. Chen, C. Liu, and F. Min, "DFT study on the adsorption of monomeric hydroxyl aluminum on Fe (II)/Mg replacement kaolinite (001) surfaces". ACS Omega, vol. 7, no. 44, pp. 39662-39670. Nov. 8, 2022. https://doi.org/10.1021/acsomega.2c03087.

[17] D. S. Lambert, and D. D. O'Regan, "Use of DFT+ U+ J with linear response parameters to predict non-

magnetic oxide band gaps with hybrid-functional accuracy". Phys. Rev. Res., vol. 5, no. 1, pp. 013160, Mar. 2023. https://doi.org/10.1103/PhysRevResearch.5.013160.

[18] X. Zhang, D. Wang, H. Nagaumi, Y. Zhou, W. Yu, X. Chong, and H. Zhang, "Morphology, thermal stability, electronic structure and mechanical properties of α-AlFeMnSi phases with varying Mn/Fe atomic ratios: Experimental studies and DFT calculations". J. Alloys Compd., Volume vol 901, pp 163523, 25 April 2022, https://doi.org/10.1016/j.jallcom.2021.163523.

[19] J. P. Perdew, K. Burke, M. Ernzerhof, "Generalized Gradient Approximation Made Simple, Phys. Rev. Lett. Vol 77, pp 3865–3868. 1996. https://doi.org/10.1103/PhysRevLett.77.3865.

[20] D. Vanderbilt, "Soft self-consistent pseudopotentials in a generalized eigenvalue formalism", Phys. Rev. B, vol. 41, pp. 7892–7895, 1990. https://doi.org/10.1103/PhysRevB.41.7892.

[21] C. G. Broyden, "The convergence of a class of double-rank minimization algorithms", IMA J. Appl. Math., vol. 6, pp. 76–90, 1970. https://doi.org/10.1093/imamat/6.1.76.

[22] A. Jain, J. Montoya, S. Dwaraknath, N. E. R. Zimmermann, J. Dagdelen, M. Horton, P. Huck, D. Winston, S. Cholia, S. P. Ong, and K. Persson, "The materials project: Accelerating materials design through theory-driven data and tools". In Handbook of Materials Modeling: Methods: Theory and Modeling. Cham: Springer International Publishing, pp. 1751-1784, 2020. https://doi.org/10.1007/978-3-319-42913-7_60-1.

[23] H. J. Monkhorst, J.D. Pack, "Special points for Brillouin-zone integrations", Phys. Rev. B 13, pp. 5188–5192, 1976. https://doi.org/10.1103/PhysRevB.13.5188.

[24] U. von Barth, L. Hedin, "A local exchange-correlation potential for the spin polarized case", J. Phys. C: Solid State Phys. Vol 5 pp 1629–1642. 1972. https://doi.org/10.1088/0022-3719/5/13/012.

[25] O. Gunnarsson, B. I. Lundqvist, "Exchange and correlation in atoms, molecules, and solids by the spin-density-functional formalism", Phys. Rev. B vol 13, no 10, pp 4274–4298. 1976. doi:10.1103/PhysRevB.15.6006.3.

[26] P. Giannozzi et al., "QUANTUM ESPRESSO: a modular and open-source software project for quantum simulations of materials", J. Phys.: Condens. Matter J. Phys.: Condens. Matter vol 21 395502 (19pp). 2009. https://doi.org/10.1088/0953-8984/21/39/395502.

[27] S. L. Dudarev et al., "Electron-energy-loss spectra and the structural stability of nickel oxide: An LSDA+U study", Phys. Rev. B vol 57, pp. 1505–1509, 1998. https://doi.org/10.1103/PhysRevB.57.1505.

[28] R. Hoffmann, "How Chemistry and Physics Meet in the Solid State", Angew. Chem. Int. Ed. Engl., vol. 26, pp. 846–878, 1987. https://doi.org/10.1002/anie.19870846.

[29] R. Dronskowski, P. E. Blöchl, "Crystal Orbital Hamilton Populations (COHP): energy-resolved visualization of chemical bonding in solids", J. Phys. Chem., vol. 97, pp. 8617–8624, 1993. https://doi.org/10.1021/j100135a014.

[30] G. Kresse, J. Furthmüller, "Efficient iterative schemes for ab initio total-energy calculations using a plane-wave basis set", Phys. Rev. B, vol. 54, pp. 11169–11186, 1996. https://doi.org/10.1103/PhysRevB.54.11169.

[31] Q. Zeng, J. Xie, J. Zhu, J. Yin, and W. Zhu, "Structural Distortion and Optoelectronic Signatures in Metal-Substituted Kaolinite: A First-Principles Investigation". Minerals, vol. 15, no. 5, pp 541 2025. https://doi.org/10.3390/min15050541.

[32] Y. Zhou, G. Lv, S. Huo, X. Yang, M. Liu, L. Wang, and L. Liao, "Selective Adsorption of Magnesium Ions and Structural Reconstruction in Acidified Palygorskite". Am. Mineral September 11, 2025. https://doi.org/10.2138/am-2025-9834.

[33] Y. Feng, H. Shi, L. Liu, X. Zhang, and D. Liu, "Functional Materials for Rare-Earth Element Recovery from Secondary Sources: A Mini Review of Adsorption-Based Strategies". Ind. Eng. Chem. Res., vol. 64, no. 50, pp. 23795-23809. Dec. 2025. https://doi.org/10.1021/acs.iecr.5c01611.

[34] Y. L., Tao, J., Gao, Q. J., Liu, and Z. T. Liu, "Structural, elastic, electronic, and optical properties of NaAlSi3O8 and Al4 [Si4O10](OH) 8 from first-principles calculations". J. Mol. Model, vol 29, no 4, 111. 2023. https://doi.org/10.1007/s00894-022-05191-y.

[35] M. W. Ibrahim, Y. Khane, Y. T. Mahmood, A. Schulz, and H. Kosslick, "Mesoporous aluminosilicate materials supported zinc oxide photocatalytic degradation of pharmaceutical pollutants". D&WT, vol 320, pp 100588. 2024. https://doi.org/10.1016/j.dwt.2024.100588.

[36] L. Wang, and J. Wu, "A review of recent progress in silver silicate-based photocatalysts for organic pollutant degradation". Inorg. Chem. Commun., vol. 129, pp. 108619. 2021. https://doi.org/10.1016/j.inoche.2021.108619.

[37] W. Li, C. F., Walther, A., Kuc, and T. Heine, "Density functional theory and beyond for band-gap screening: performance for transition-metal oxides and dichalcogenides". J. Chem. Theory Comp., vol. 9, no. 7, pp. 2950-2958, August 22, 2013. https://doi.org/10.1021/jp9536312.

[38] S. Kapse, M. Voccia, F. Viñes, and F. Illas, "Chemical bonding and electronic properties along Group 13 metal oxides".J. Mol. Model, Vol 30, no 6, pp 161. 2024. https://doi.org/10.1007/s00894-022-05191-y.

[39] A. Togo, “First-principles phonon calculations with phonopy and phono3py”. J. Phys. Soc. Jp. vol 15; no 92(1):012001. Jan 2023. https://doi.org/10.7566/JPSJ.92.012001.

[40] K. K. Pandimeena, M. C. Robert, and S. Saravanakumar, “Energy gap tuning, ferromagnetic switching, visualization of electron density and bonding in dilute magnetic semiconductor Fe-doped SnO_2”. Optik., vol. 1, no. 287 pp. 171091, Sept, 2023 https://doi.org/10.1016/j.ijleo.2023.171091.

[41] C. W. Castleton, A. Höglund, and S. Mirbt. “Density functional theory calculations of defect energies using supercells”. MSMSE, vol. 17, no. pp. 084003, Dec, 2009. https://doi.org/10.1088/0965-0393/17/8/084003.